1,3-Diphenylisobenzofuran: a Model Chromophore for Singlet Fission

Justin C. Johnson
National Renewable Energy Laboratory, 15013 Denver West Pkwy, Golden, CO 80401

and Josef Michl,
Department of Chemistry and Biochemistry, University of Colorado, 215 UCB, Boulder, CO 80309-0215, and Institute of Organic Chemistry and Biochemistry, Academy of Sciences of the Czech Republic, Flemingovo nám. 2, 16610 Prague 6, Czech Republic, Josef.Michl@colorado.edu, 303-492-6519

Abstract

After an introductory description of the singlet fission phenomenon, the ground and electronically excited states of the parent 1,3-diphenylisobenzofuran chromophore (**1**) and about a dozen of its derivatives are described. A discussion of singlet fission in thin polycrystalline layers of these materials follows. The highest quantum yield of triplet formation by singlet fission, 200% at 80 K, is found in one of the two known crystal modification of the parent. In the other modification and in many derivatives, excimer formation competes successfully and triplet yields are low. Solution photophysics of covalent dimers is described next. Triplet yields are very low, but interesting phenomena are uncovered. One is an observation of a separated-charges (charge-transfer) intermediate in highly polar solvents. The other is an observation of excitation isomerism in both singlet and triplet states, where in one isomer the excitation is delocalized over both halves of the covalent dimer, whereas in the other it is localized on one of the halves. Finally, the operation of a simple device illustrating the use of triplets generated by singlet fission for charge separation is presented.

Keywords

1,3-diphenylisobenzofuran; photophysics, solar energy, singlet fission, covalent dimers

Introduction

Singlet fission (SF) is of interest for the conversion of solar energy into electricity or fuel, since a suitable combination of an ordinary with an SF sensitizer should increase the efficiency of a single-junction solar cell. For the production of electricity, the theoretical efficiency rises from the Shockley-Queisser limit of ~32% [1] to ~46% [2]. Before describing SF in solids containing 1,3-diphenylisobenzofuran (**1**) and its derivatives, analogs, and covalent dimers, we provide a brief introduction to the phenomenon. Additional detail can be found in review articles [3,4,5], and in an earlier review dealing specifically with **1** [6].

SF is a process in which a singlet excited chromophore transfers some of its energy to a neighboring chromophore and both end up as triplets. The triplets are initially coupled into an overall singlet, making the process spin-allowed and possibly very fast. Figure 1 shows the energy levels of two chromophores, one on the left and the other on the right, and the initial singlet excitation of the left chromophore, normally by absorption of a photon (process 1). The SF event, the production of a triplet state on each chromophore, is shown as process 2. The description is oversimplified in that the initial excitation may be shared by more than one molecule.

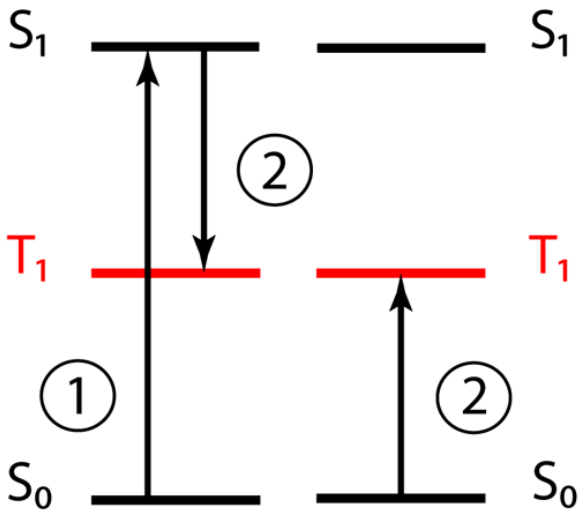

Figure 1. Singlet excitation (1) followed by SF (2). Reprinted with permission from reference 3. Copyright 2010 American Chemical Society.

Properly speaking, SF is not over until the two resulting triplets have separated and become independent, and this is not shown in Figure 1. It requires overcoming any binding energy between them, which typically appears to be small if the chromophores are located in two distinct molecules. The separation often happens rapidly when the chromophores occur in the form of crystals, aggregates, or polymers, where triplet hopping from molecule to molecule is generally facile, or even in solution, where solute molecules can diffuse apart. If the binding energy of the two triplets is sufficiently large, the bound triplet pair (biexciton) might be separately observable and kinetically significant, in which case the total SF process would be a two-step event. In isolated covalent

dimers, the separation cannot occur and the process stops after step 2 in Figure 1, making such dimers a somewhat special case.

A simplified schematic representation of the critical step 2 of Figure 1 in the diabatic representation is provided in Figure 2 and we shall see below that in principle it itself also could occur in a single step or in two. The final separation of the two triplets will not be discussed here.

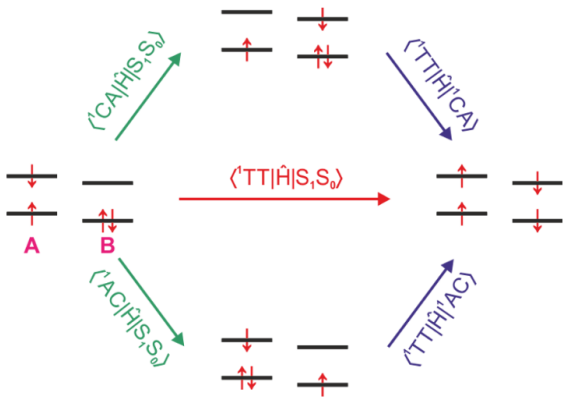

Figure 2. A schematic representation of SF paths (see text).

Figure 2 is only symbolic in that it shows the dominant electron configurations but in fact others contribute as well. The left-hand side shows frontier orbital occupancies and spins in the initial singlet state with the left chromophore singly excited and the right chromophore in its ground state. This initial state is normally prepared by absorption of a photon (in reality, the singlet excitation is often shared by several molecules). The right-hand side shows frontier orbital occupancies and spins after SF has taken place. In the resulting doubly excited state of the dimer (biexciton) each chromophore is in its triplet state, but the two triplets are at first coupled into an overall singlet. Again, the real situation is more complicated since a combination of two triplets gives rise to nine substates and spin-dependent parts of the interaction Hamiltonian cause the initially reached singlet to develop in time, giving rise to magnetic field effects that are one of the hallmarks of SF [7] but will not be discussed here.

There are two ways (mechanisms) in which step 2 can proceed. The usual mechanism is single-step with no intermediate. Its rate is proportional to the square of a Hamiltonian matrix element that in the present approximation contains only three contributions. A small one is due to a direct interaction of the initial with the final configuration and is indicated by a red arrow in Figure 2. Two large ones, possibly of mutually opposite signs, are due to mediated interactions indicated by cyan and blue arrows. The two mediating states that provide the interaction (superexchange) paths are the charge-transfer configurations shown in Figure 2 at the top and at the bottom. In these, an electron has been removed from one or the other chromophore and added to its partner. Although there still is some debate as to whether the direct or the mediated contribution to the matrix element is more important, to our knowledge in all cases in which the two have been carefully separated in a computation the direct contribution was found to be negligible relative to the algebraic sum of the mediated ones. The possibly destructive interference between the two mediated paths has interesting implications for the dependence of the matrix element on the choice of the mutual disposition (distance and orientation) of the two chromophores if they are identical and we return to it below.

It can be largely avoided if the two chromophores are different and one acts as an electron donor and the other as an electron acceptor.

In rare instances the energy of one or both charge-transfer configurations can be so favorable that they no longer represent virtual states but become observable real states with finite lifetimes (minima in the lowest excited singlet hypersurface). Then, process 2 in Figure 1 can proceed by a two-step mechanism with a charge-transfer species as an observable intermediate. We shall see below that certain covalent dimers of **1** dissolved in highly polar solvents are good candidates for this two-step mechanism.

SF was initially observed in crystals, and the first report was for anthracene [8]. It was subsequently invoked to explain thermal quenching of photoexcited fluorescence in tetracene [9]. The phenomenon was confirmed beyond doubt by further studies of tetracene and pentacene [10,11,12,13,14,15,16,17,18] and was thoroughly reviewed [19]. Additional studies of polyacene crystals followed [20,21,22,23,24,25,26,27,28]. Once the process was considered well established, interest in it abated. Its was found in a few other compounds, also non-crystalline ones such as carotenoids and conjugated polymers, and in solution for a molecule composed of two tetracenes connected through a covalent bridge [29,30], but the yields of triplets formed in these additional structures were mostly just a few percent and always below 30-35%. SF thus acquired the reputation of a rare and generally inefficient process. The exceptions were tetracene and pentacene, which were suspected to give very high triplet yields, although the actual numbers were not known.

When it comes to potential practical utility, triplet yields that lie substantially below the theoretical upper limit of 200%, and certainly those below 100%, are of no interest. SF materials need to meet a large number of additional conditions, among which stability in the sun under small amounts of atmospheric oxygen is the most obvious. This requirement eliminates both parent tetracene and pentacene but leaves the hope that some of their analogs and derivatives might be acceptable.

The pioneering studies firmly established the existence of the SF process and recognized that it is favored in materials in which the first singlet excitation energy $E(S_1)$ is roughly equal to twice the first triplet excitation energy $2\ E(T_1)$, as in tetracene and pentacene. However, it was only the realization by Nozik and his collaborators [2] that SF could be extremely helpful in boosting solar cell efficiency that launched the present wave of interest in the phenomenon. Until then, there was little motivation to design and then synthesize sturdy and light-fast chromophores whose dimers, oligomers, or crystals would be optimized for high triplet yields from SF. In 2009-2010, several reports of highly efficient SF materials appeared [31,32,33,34] and led to a thorough reinvestigation of the phenomenon. After a decade of effort, there now is general consensus that efficient SF indeed is rare, but that under the right circumstances, the triplet yield can actually be very close to 200%, as is the case in the two champions, tetracene and pentacene. We believe now, as we did then, that finding a similar yield in a material that is actually practically useful needs to be the top priority in SF research.

The first paper that addressed the issue of chromophore design for optimal SF appeared in 2006 and used simple theoretical considerations to identify two partially overlapping classes of likely candidates among the vast number of possibilities: large alternant hydocarbons and biradicaloids [35]. One of the biradicaloid structures identified as promising was **1** (Figure 3), a compound of previously known [36,37] triplet energy, already in use for some time for the detection of singlet oxygen [38,39]. This is the species to which the present chapter is dedicated. It is the first and to date the only highly efficient structure entirely different from the traditional polyacenes that was

chosen rationally for SF investigations. It is even less practically useful than tetracene and pentacene themselves. Not only is it sensitive to the combination of light and air, it also does not absorb far enough into the visible. However, its properties prove that a rational design is possible, and it represents an interesting model chromophore. Numerous derivatives of **1**, shown in Figure 2, are synthesized much more easily than those of tetracene and pentacene, and so are its covalent dimers.

Subsequent work elaborated the role of biradicaloid character in the chromophore farther [40]. Various specific biradicaloid structures have been proposed [41,42,43], but only very few have been tested and none of those have shown a high efficiency so far. The requirement of biradicaloid character is somewhat unfortunate from a practical point of view, since most known biradicaloids are fairly unstable. By far most of the hundreds of SF studies published in the last decade have been devoted to detailed understanding of the SF process in the higher polyacenes, and to examination of substituted and otherwise modified tetracenes and pentacenes. Although interesting and important, they lie outside the scope of the present chapter.

The other urgent and difficult issue to address in the search for SF materials is the optimal mutual disposition of the chromophores in a crystal, aggregate, oligomer, or dimer [44]. This problem is difficult, because already the space of mutual disposition of a pair of rigid bodies is six-dimensional, and the dimensionality gets out of hand rapidly for larger sets of chromophores. The challenge was first addressed tentatively in 2010 [3]. A simple old model that only considers the highest occupied (HOMO) and the lowest unoccupied (LUMO) molecular orbital on each partner in a pair was selected (Figure 2), simple formulas for the SF matrix element were worked out, and it was suggested that a slip-stacked geometry of two planar π-electron systems was especially favorable, whereas the exactly stacked geometry was not. In calculations that are not limited to the HOMO and LUMO orbitals, the contrast is less stark, but the slip-stacked geometry is still favored [45]. The size of this matrix element is critical, since in the Fermi golden rule approximation the rate of SF is proportional to its square.

As noted above, in the HOMO/LUMO model, the matrix element for SF consists of the 'direct' term and the 'mediated' terms, which involve virtual charge transfer between the two members of a pair [3]. Although it was not clear at first which of these contributions to the matrix element is dominant, so far, in all computations in which the terms were carefully separated the mediated one dominates overwhelmingly[46]. We believe that in most cases it is the only one that needs to be considered seriously.

Further simplification of the HOMO/LUMO model has yielded an extremely simple approximate formula for the SF matrix element [47] that requires only the knowledge of coefficients of the frontier MOs and the overlaps of the atomic orbitals on one and the other partner. It permits a computer search for local maxima in the six-dimensional space at hundreds of millions of dimer geometries in a few hours or days, depending on chromophore size.

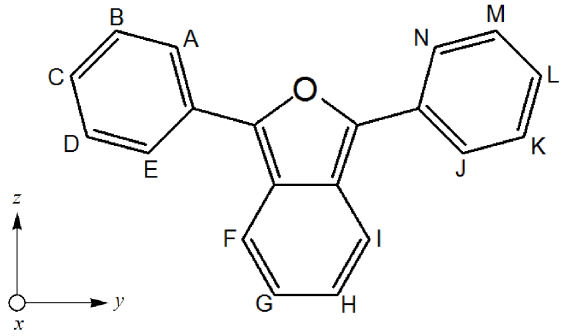

1

cmpd	A	B	C	D	E	F	G	H	I	J	K	L	M	N
1	H	H	H	H	H	H	H	H	H	H	H	H	H	H
1a	H	H	F	H	H	H	H	H	H	H	H	H	H	H
1b	H	H	F	H	H	H	H	H	H	H	H	F	H	H
1c	F	H	F	H	F	H	H	H	H	H	H	H	H	H
1d	F	F	F	F	F	H	H	H	H	H	H	H	H	H
1e	F	F	F	F	F	H	H	H	H	F	F	F	F	F
1f	H	H	CH_3	H	H	H	H	H	H	H	H	H	H	H
1g	H	H	*t*-Bu	H	H	H	H	H	H	H	H	H	H	H
1h	H	*t*-Bu	H	*t*-Bu	H	H	H	H	H	H	H	H	H	H
1i	H	H	C_2H_3< (polymer)	H	H	H	H	H	H	H	H	H	H	H
1j	N	H	H	H	H	H	H	H	H	H	H	H	H	H
1k	MeN^+OTf^-	H	H	H	H	H	H	H	H	H	H	H	H	H
1l	H	$MeN^+PF_6^-$	H	H	H	H	H	H	H	H	H	H	H	H
1m	H	H	MeN^+OTf^-	H	H	H	H	H	H	H	H	H	H	H
1n	H	H	$(CH_2)_5COOH$	H	H	H	H	H	H	H	H	H	H	H

Figure 3. Formulas of 1,3-diphenylisobenzofuran (**1**) and its derivatives.

For a pair of ethylene molecules taken as the simplest model, a few dozen best geometries were identified in this manner, but only a few of these offer really large matrix elements [5]. The simplicity of the formula allows the formulation of a design rule by inspection, and the rule is indeed satisfied in the favorable structures found by the computer: one of the π-symmetry atomic orbitals (AOs) on the first ethylene needs to overlap with both π-symmetry AOs of the second ethylene, while the second AO on the first ethylene should not overlap with the AOs of the second ethylene at all or at least as little as possible. A generalization of this simple rule applies to more complicated chromophores [5].

In the Fermi golden rule approximation, both the just discussed electronic matrix element and a density of states term are important. In the Marcus theory approximation, the latter can be expressed through reorganization energy and reaction exoergicity, which requires a consideration of the possible differences between excitation energies in an isolated chromophore and those in a

dimer (exciton splitting) or a crystal (Davydov splitting). Simple approximate formulas have been developed for the dimer case and added to the computer program that automatically finds optimal geometries in the six-dimensional space of dimer geometries, permitting a removal of some geometries that appear favorable on the basis of the electronic matrix element alone [5].

Maximizing the rate of SF represents only one half of the task at hand. The other half is minimizing the rates of competing processes. Intramolecular competing processes such as intersystem crossing, internal conversion, and unimolecular photochemical reactions (e.g., cis-trans isomerization) are relatively easy to avoid by a suitable choice of the chromophore used. It is more difficult to avoid intermolecular processes that need to be considered as soon as a crystal, aggregate, or a dimer are used. The most important of these are the formation of excimers and charge-separated states; intermolecular photochemical reactions can usually be avoided by a suitable choice of chromophores. Both excimer formation and charge separation are detrimental even though their formation preserves most of the electronic excitation energy and does not necessarily preclude subsequent SF (cf. the two-step mechanism described above). In practice, however, they represent the most common threat to high efficiency in SF. First, they lower the energy of the excited singlet state, making it less likely that the formation of two triplets will be exoergic. Second, in their lowest energy electronically excited state, excimers may have a smaller matrix element for SF. Third, both excitons and charge-separated states often have efficient channels for internal conversion to the ground or the lowest triplet state (e.g., intersystem crossing in the charge-separated species). We shall see below that in the case of **1** and its derivatives that is of interest presently, formation of excimers is often competitive and lowers the yield of triplets from SF. Since it may require motion within the crystal, its occurrence is not easy to predict.

At present, efforts are underway to identify favorable geometries in pairs of chromophores other than the simple ethylene model[5], including **1**. Although the project has not yet been completed, it has become clear that the results are quite sensitive to minor changes in dimer geometry, and we shall see below that indeed the two known crystal structures of **1**, although quite similar, provide very different triplet yields from SF [48]. Thus, even though the structure of **1** was selected for investigation in a rational way based on first principles, it was only sheer luck that in the initially investigated polycrystalline layers [32] **1** was packed in the crystal form that provides triplet yields close to 200%.

It needs to be emphasized that in real crystals electronic excitation can be delocalized over several chromophores and that entropy needs to be considered. The correct description of SF then becomes considerably more complicated than in a dimer [49]. The structural guidance obtained from theoretical work on dimers should therefore be viewed as only approximate.

Synthesis of 1, its Analogs and Derivatives

The classical synthetic approach to **1** and similar compounds is the reaction of a 3-arylphthalide with an aryllithium (Figure 4). It has been recently used for the syntheses of a series of alkylated [50] and fluorinated[51] derivatives for SF studies (Figure 3), to be discussed next. It has also been used for the preparation of numerous covalent dimers [52], which will be discussed below. Another synthetic approach has been described more recently [53] and the parent **1** is available commercially.

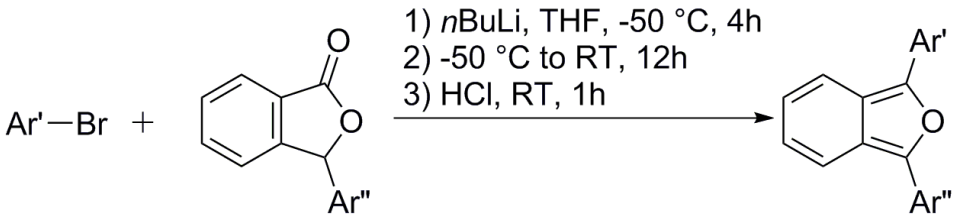

Figure 4. The standard synthetic route to **1** and its derivatives.

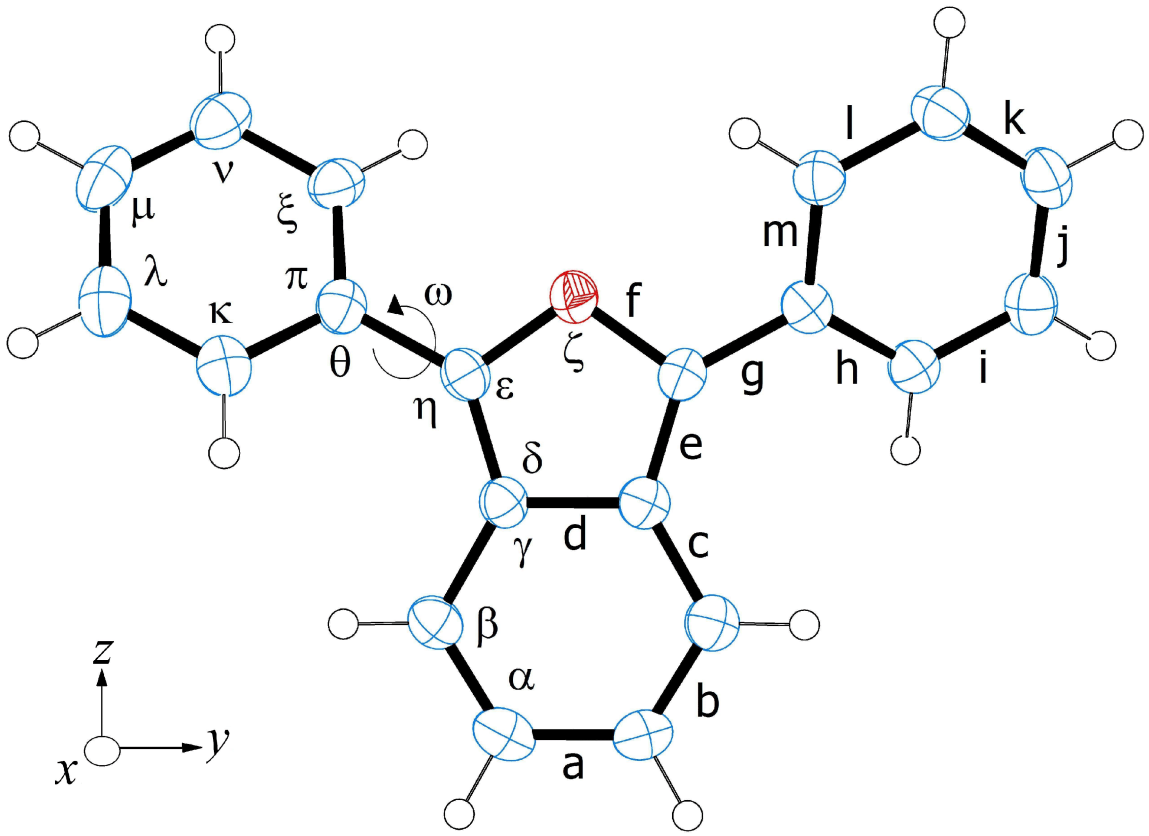

	a	b	c	d	e	f	g	h
exp	1.421	1.379	1.415	1.444	1.398	1.37	1.443	1.406
RI-CC2/TZVPP	1.430	1.357, 1.353	1.422, 1.427	1.445	1.378, 1.375	1.375, 1.374	1.461, 1.459	1.392, 1.395
	i	**j**	**k**	**l**	**m**	**α**	**β**	**γ**
exp	1.393	1.396	1.397	1.391	1.407	121.5	118.4	120.1
RI-CC2/TZVPP	1.385, 1.386	1.380, 1.375	1.383, 1.389	1.394, 1.383	1.394, 1.389	121.5, 121.9	118.8, 118.7	119.7, 119.5
	δ	**ε**	**ζ**	**η**	**θ**	**κ**	**λ**	**μ**
exp	106.6	108.4	110	134.8	120.6	120.4	120.4	119.5
RI-CC2/TZVPP	106.4, 106.9	109.0, 108.9	108.7	135.2, 135.5	120.8, 121.0	120.6, 120.4	120.4, 120.4	119.7, 119.8
	ν	**ξ**	**π**	**ω**				
exp	120.5	120.4	118.9	23.5				
RI-CC2/TZVPP	120.2, 119.9	120.2, 121.0	118.8, 118.5	23.8, 24.2				

Figure 5. Ground-state structure of the C_2 conformer of **1** from single-crystal X-ray diffraction (ellipsoids drawn at 50%) and from calculation. Reprinted with permission from reference 54. Copyright 2010 American Chemical Society. Distances in Å, angles in degrees.

Electronic States of Parent 1 and its Ions

Much is known about solution spectroscopy, photophysics, and oxidation-reduction behavior of the isolated molecule of the parent chromophore **1**, its radical cation, and its radical anion [54].

Table 1. Optimized RICC2/TZVPP geometries of excited and ionized states of the C_2 conformer of **1**, state symmetries in the C_2 group, and experimental geometry of the S_0 ground state (see Figure 5 for the definition of geometrical parameters) [54].

Parameter	S_0 (A)	S_1 (B)	S_2 (A)	T_1 (B)	D^+ (A)	D^- (B)
a	1.421	1.388	1.433	1.380	1.410	1.400
b	1.379	1.414	1.403	1.418	1.388	1.392
c	1.415	1.402	1.391	1.388	1.405	1.412
d	1.444	1.442	1.473	1.432	1.427	1.431
e	1.398	1.421	1.438	1.440	1.418	1.410
f	1.370	1.389	1.378	1.398	1.367	1.385
g	1.443	1.415	1.412	1.410	1.428	1.419
h	1.406	1.418	1.423	1.420	1.400	1.412
i	1.393	1.387	1.391	1.387	1.374	1.376
j	1.396	1.400	1.397	1.400	1.387	1.390
k	1.397	1.400	1.408	1.400	1.388	1.391
l	1.391	1.387	1.385	1.386	1.373	1.374
m	1.407	1.421	1.419	1.422	1.401	1.415
α	121.5	121.4	120.9	120.9	121.4	121.1
β	118.4	118.1	118.8	118.8	117.9	119.0
γ	120.1	120.4	120.2	120.3	120.6	119.9
δ	106.6	106.2	105.9	106.8	106.6	107.0
ε	108.4	110.2	108.7	109.2	108.4	108.5
ζ	110.0	107.2	110.5	108.1	109.9	109.0
η	134.8	134.4	134.6	134.7	134.8	134.8
θ	120.6	121.5	120.5	122.1	120.3	123.0
κ	120.4	120.3	120.0	120.5	119.9	121.2

λ	120.4	120.7	120.8	120.7	119.9	121.8
μ	119.5	119.6	119.6	119.4	120.7	117.6
ν	120.5	120.6	120.4	120.7	119.9	121.7
ξ	120.4	120.4	120.5	120.6	119.8	121.2
π	118.9	118.5	118.7	118.1	119.8	116.6
ω	23.5	9.9	14.0	9.1	22.7	6.7

Molecular Geometry. Steric interference between the ortho hydrogens of the phenyl substituents on the one hand and the oxygen lone pair and the peri hydrogens of the isobenzofuran core on the other hand prevents complete coplanarity and results in the existence of two ground state conformations with phenyl twist angles of about 24°, one with C_2 and the other with C_s symmetry. They are calculated to have nearly identical energies and geometries, and differ primarily only by the sense of rotation of the phenyl groups. Their calculated vibrational and electronic transition spectra are essentially identical. The crystal structure of the C_2 conformer has been solved [54] (Figure 5 and Table 1) and the alternation of CC bond lengths in its isobenzofuran core suggests that in the ground state **1** can be described approximately as a π-excessive heterocyclic polyene with four double bonds and two phenyl substituents. Calculated geometries of the S_1 and T_1 excited and D^+ and D^- radical ion states exhibit less bond length alternation in the isobenzofuran ring system, indicating stronger π-electron delocalization. This is compatible with the reduced twist angles of the phenyl substituents, which are only about 7 - 10° in the S_1, T_1, and D^- states, making the C_2 and C_s conformers nearly identical and effectively of C_{2v} symmetry. Interestingly, in the D^+ radical cation, the phenyl twist angle remains nearly the same as in the ground state.

Singlet Excited States [54]. The electronic transition moments in both conformers of the slightly non-planar **1** are calculated to lie within a few degrees of the *y* and *z* axes shown in Figure 5 and it is acceptable to describe the electronic states of **1** in terms of the C_{2v} group.

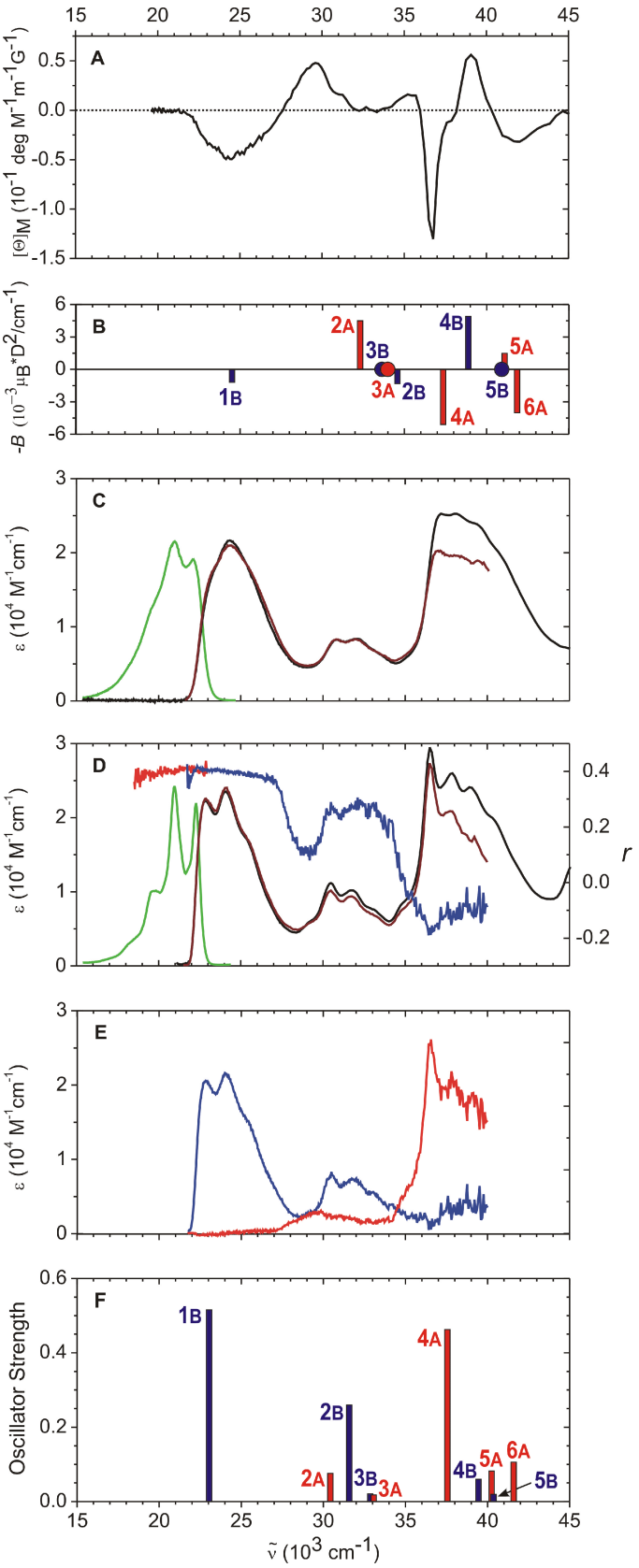
A
B
C
D
E
F
[Θ]M (10-1 deg M-1m-1G-1)
-B (10-3 μB*D2/cm-1)
ε (10^4 M-1cm-1)
r
Oscillator Strength
ν̃ (10^3 cm-1)
1B
2A
3B
3A
2B
4B
4A
5A
5B
6A

Figure 6. Spectra of **1**. A: MCD in CH (rt). B: PPP calculation. Bar height indicates the value of the B term, bar color the polarization (blue, *y*; red, *z*). C: absorption (black), fluorescence (green), and fluorescence excitation (red) in CH (rt). D: absorption (black), fluorescence (green), fluorescence excitation (red), fluorescence anisotropy (bright red), and fluorescence excitation anisotropy (blue) in 3-MP (77 K). E: Absorption in 3-MP (77 K) decomposed into its *y*-polarized (blue) and *z*-polarized (red) components. F: CC2/TZVPP calculation (all transitions have been shifted to the lower values by 3000 cm^{-1}). Bar length indicates the oscillator strength of *y*-polarized (blue) and *z*-polarized (red) transitions. Reprinted with permission from reference 54. Copyright 2010 American Chemical Society.

Panels A and C in Figure 6 show the room-temperature absorption, fluorescence, fluorescence excitation, and magnetic circular dichroism of **1** in cyclohexane (CH). Panel D shows the low-temperature (77 K) absorption, fluorescence, fluorescence excitation, and the anisotropy of fluorescence and fluorescence excitation in 3-methylpentane (3-MP). It is believed that the two conformers contribute equally to the spectra shown. Parts B and F show the results of semiempirical and ab initio calculations, both of which account well for the observations.

The photophysical data for **1** are nearly solvent-independent: the first absorption peak lies at ~24 300 cm^{-1}, is relatively intense (ε_{max} = 23400 M^{-1} cm^{-1}), and its vibronic features are spaced at ~1400 cm^{-1}. Fluorescence is an approximate mirror image of the first absorption band. Its first peak is found at ~22 100 cm^{-1}, and its quantum yield is 0.96 ± 0.03. The absence of detectable internal conversion or intersystem crossing makes **1** a favorable candidate for SF [35]. The fluorescence lifetime is ~6 ns and corresponds to a fluorescence rate constant of ~0.15 ns^{-1}. At low temperature, the vibronic structure is more pronounced and makes it clear that the true Stokes shift is small, less than 500 cm^{-1}.

The essentially constant fluorescence anisotropy of 0.38 for excitation anywhere in the first absorption band and observation anywhere in the emission demonstrates that the first absorption band and the fluorescence are purely polarized along the same axis, and all methods of calculation agree that its direction is *y* in Figure 5. The pure polarization of the first absorption band permitted the use of linear dichroism in stretched polyethylene to prove that two distinct conformers are actually present and orient to different degrees. Their Franck-Condon envelopes in the first transition are slightly different.

The second electronic transition from the ground state occurs near 28000 cm^{-1} and is *z*-polarized (Figure 6E). It is weak and cannot be seen in an ordinary absorption spectrum. The somewhat stronger broad band around 37000 cm^{-1} is due to a *y*-polarized transition, and calculations predict two additional very weak transitions near this energy, one of each polarization. The first intense z-polarized transition is found at ~37000 cm^{-1}, where a non-radiative decay channel opens and the fluorescence excitation spectrum stops following the absorption spectrum faithfully.

The absorption spectrum of the S_1 state appears immediately following resonant pulsed excitation and decays as a single exponential with the same lifetime as the fluorescence. The most prominent bands are located near 14500 and 22000 cm^{-1} (Figure 7).

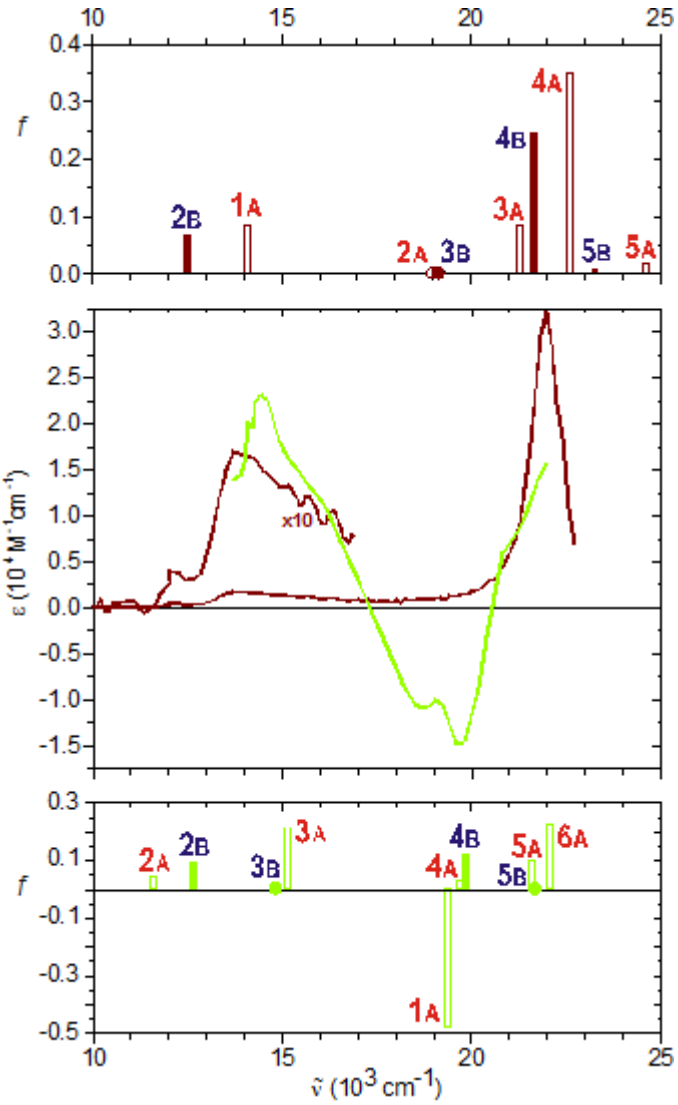

Figure 7. Transient absorption spectra of the first excited singlet (S_1, chartreuse, τ = ~5 ns) and the first triplet (T_1, brown, τ = ~230 μs) of **1** in DMSO. Reprinted with permission from reference 54. Copyright 2010 American Chemical Society.

The nature of the excited states and of the molecular orbitals involved in the excitations is shown in Figure 8. The lower energy states can be understood simply in terms of the perimeter model [55,56], which allows the S_1 state to be given the label L_1 and the S_2 state, the label L_2. The perimeter model also leads to a recognition of **1** as a "positive hard MCD chromophore" [57], and correctly accounts for signs in the MCD spectrum.

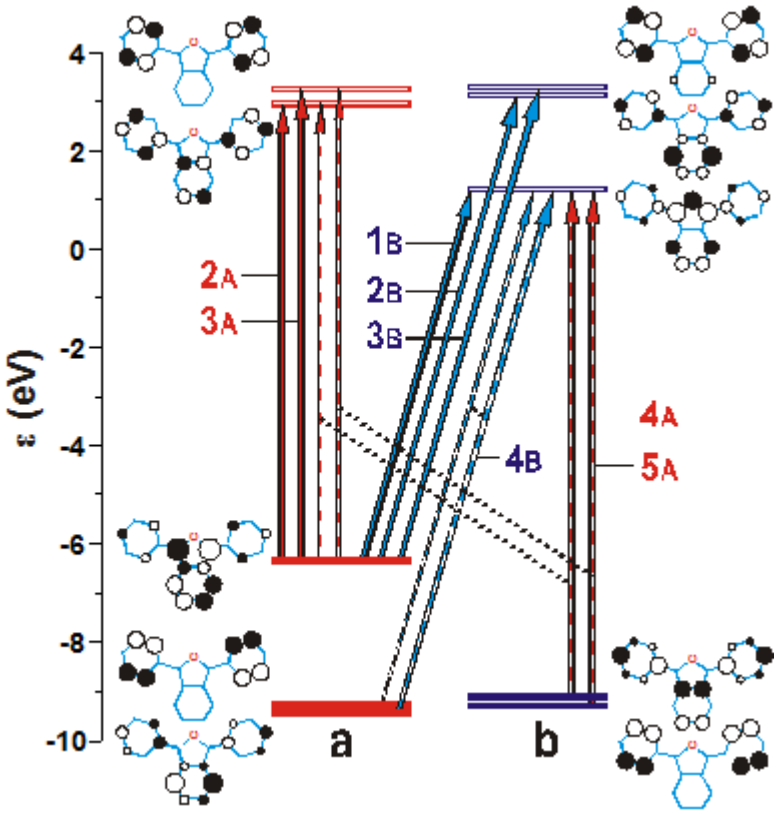

Figure 8. Orbital energies in **1**. Chief contributions to $S_0 \rightarrow S_x$ excitations calculated at the CC2/TZVPP level are shown. Striped arrows indicate that more than one electron promotion has a significant amplitude. Reprinted with permission from reference 54. Copyright 2010 American Chemical Society.

Triplet States. As might be expected from a fluorescence quantum yield of nearly unity, no phosphorescence is observed in a low-temperature glass, and no transient triplet-triplet absorption is seen in a laser flash photolysis experiment without a sensitizer. The excitation energy of T_1 has been reported as ~11 900 cm^{-1} (adiabatic) in benzene solution based on triplet sensitization [36], as ~12 900 cm^{-1} in DMF based on electrogenerated chemiluminescence [37], and ~11 400 cm^{-1} in a solid film from electron energy loss spectrum [54]. Triplet transitions T_1-T_n were identified by diffusion-controlled energy transfer from the triplet of photoexcited anthracene to ground state **1** (Figure 7). A strong and narrow band at ~21500 cm^{-1} has been attributed to overlapping transitions from the 1B lowest triplet state to the 3A, 4B, and 4A states, and should therefore be of mixed polarization. Lower lying triplet transitions are calculated and observed near 14000 cm^{-1} but are considerably weaker than those at higher energy. The triplet lifetime in dilute solution is ~230 μs.

The most important gap in our knowledge is the absence of the EPR spectrum of the triplet of **1**, which means that the *D* and *E* parameters ordinarily used for the description of the zero-field-splitting tensor are unknown.

In summary, the vertical excitation energies S_0 - S_1 (~24 300 cm^{-1}), S_0 - T_1 (~11 400 cm^{-1}), and S_0 - T_2 (estimated at 25 500 cm^{-1}) satisfy the conditions $E(S_1)$, $E(T_2) \geq 2\ E(T_1)$, considered desirable for SF.

Electrochemistry and Radical Ions. As would be expected for a π-excessive heterocycle, **1** is relatively easy to oxidize and difficult to reduce. In liquid SO_2, reversible one-electron oxidation takes place at +0.35 V against ferrocene/ferricinium ($Fc^{0/1}$), +0.85 V against a saturated calomel electrode (SCE). Reversible one-electron reduction in *N*,*N*-dimethylformamide takes place at -1.85 V against SCE [52].

The absorption spectra of the radical cation $\mathbf{1}^{+\bullet}$ and radical anion $\mathbf{1}^{-\bullet}$, produced by pulse radiolysis in DCE and THF solution, respectively, are shown in Figure 9, revealing bands at 15000 cm^{-1} and 18500 cm^{-1}, respectively. As might be expected [58], the transitions in the absorption spectra of the singlet and triplet states of **1** and of the radical ions $\mathbf{1}^{+\bullet}$ and $\mathbf{1}^{-\bullet}$ are inter-related.

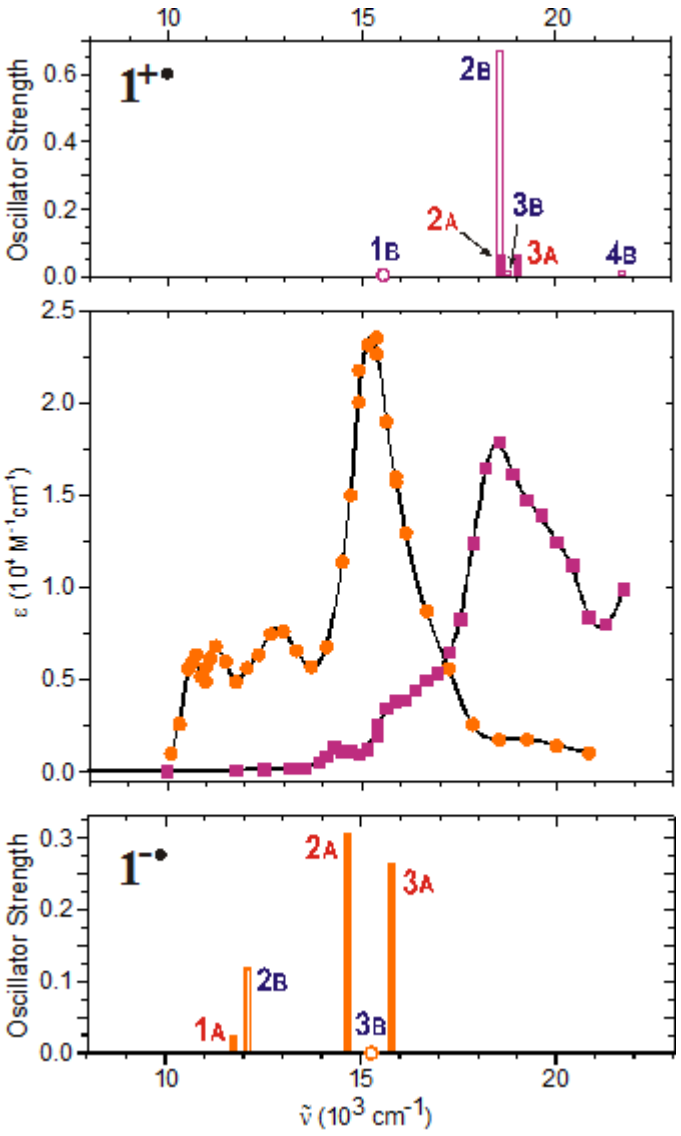

Figure 9. Absorption of the radical anion $\mathbf{1}^{-\bullet}$ (●) and radical cation $\mathbf{1}^{+\bullet}$ (■) obtained by pulse radiolysis of 5 mM **1** in THF and DCE, respectively. CC2/TZVPP calculated spectra on top (cation) and bottom (anion). Full bars: *z* polarization, empty bars: *y* polarization. Calculated transitions have been shifted to the lower energies by 3000 (cation) or 2000 (anion) cm^{-1}. Reprinted with permission from reference 54. Copyright 2010 American Chemical Society.

Substituted Derivatives. Various derivatives of **1** carrying weakly interacting substituents have been synthesized (Figure 3), mostly with the intention of keeping the chromophore nearly the same but modulating its packing in the solid state dramatically. Measurements of SF rates would then presumably primarily provide information on the effect of crystal packing alone. In solution, the optical properties primarily reflect the degree of twisting of the phenyl groups that the

substitution engenders. For the fluorinated derivatives, the twisting increases when fluorine atoms are present at the ortho or meta positions in the phenyl groups, whereas substitution in the para position has negligible effect. A larger twist reduces conjugation and causes a blue shift in the onset of absorption and fluorescence. As the degree of fluorination increases, the fluorescence lifetimes and quantum yields are slightly reduced. The triplet spectra are largely unaffected. For the alkyl derivatives **1f -1h**, the deviations of absorption spectra from **1** are minor. All derivatives show a slight red shift of less than 200 cm^{-1} and remain highly fluorescent.

Photophysics of Thin Films of 1 and Its Derivatives

Thin films of **1** have been fabricated using thermal evaporation of powdered material or casting from solution [32]. The films employed for photophysical measurements were between 25 and 150 nm thick. They tend to be highly polycrystalline as judged by sharp and strong X-ray diffraction (XRD) peaks, but the crystal structure depends on the deposition conditions. Two dominant progressions of XRD peaks are seen, separated by about 0.1° at the first observable reflection ($2\theta = \sim 9°$), Figure 10A. The films with lower 2θ values are labeled α and those with higher 2θ values are labeled β. Films of a mixed type can be made directly or through strategic annealing steps. Rapid deposition of **1** (> 5 Å/s) favors the polymorph α, whereas slower deposition and mild thermal annealing favor the β form. Most solution cast films were of the α form, but exposure to ambient conditions converted them to β. Crystal views are shown in Figure 10B. Crystals grown from solution were isolated and studied with XRD and structural analysis. Two forms were discovered, matching the forms seen in thin films [48]. The crystal habits also roughly match crystallite shapes observed via atomic force microscopy for thin films. The ability to fabricate films of nearly pure polymorph composition and to compare with known bulk structures was a major milestone for the pursuit of understanding the role of interchromophore coupling on SF [44]. The use of naturally occurring polymorphs in this fashion has become common among other SF systems [59,60].

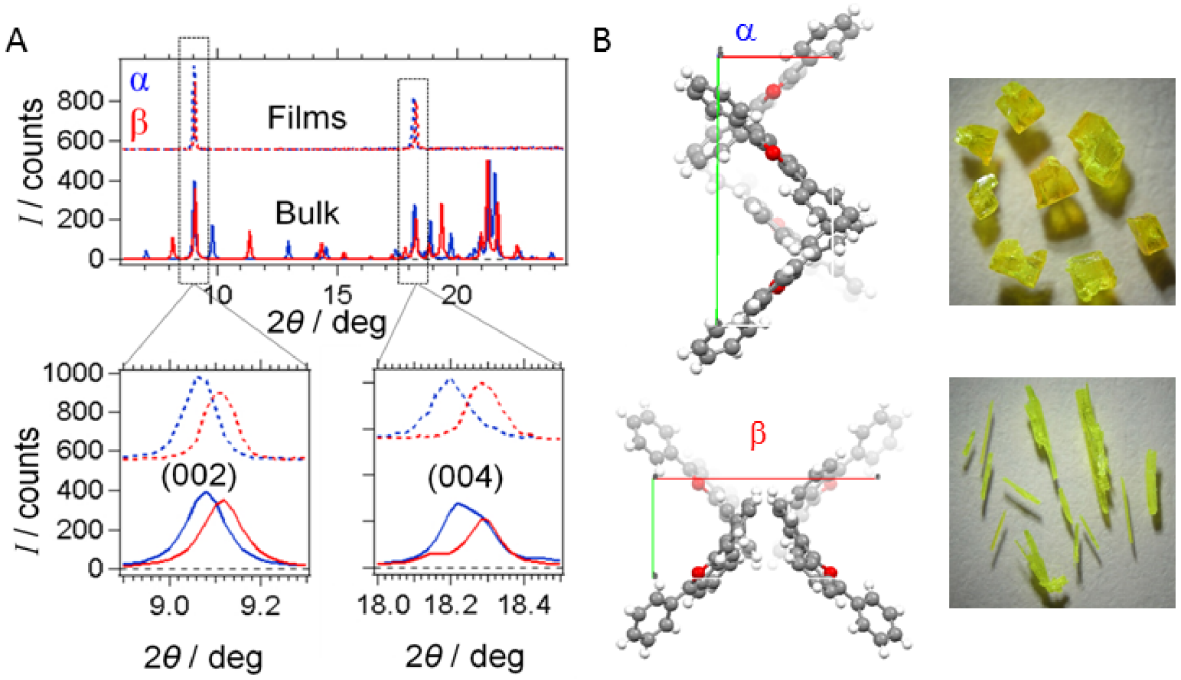

Figure 10. A: XRD of two thin film types of **1**. B: Unit cells of α and β thin films looking down the *c* axis and photographs of their respective single crystals.

Despite the similarity of the unit cell parameters and nearest neighbor interactions, the two film types exhibit very different photophysics. Ground state absorption is best judged by extracting absorbance from integrating sphere measurements of transmission and reflection due to considerable scattering and wavelength-dependent reflectivity of the thin films. The resultant spectra are shown in Figure 11A. They are shifted to the red of those of isolated **1** by 300 cm^{-1} and 1000 cm^{-1} for α and β, respectively. The vibronic envelopes are also altered, with the α form possessing a larger amplitude for the 0-1 vibronic transition. The fluorescence retains a similar vibronic progression for both film types, but also contains an underlying red-shifted Gaussian band (Figure 11B). This feature is stronger for β than for α film types, as is the overall room-temperature fluorescence yield, 59% vs. 16%, respectively.

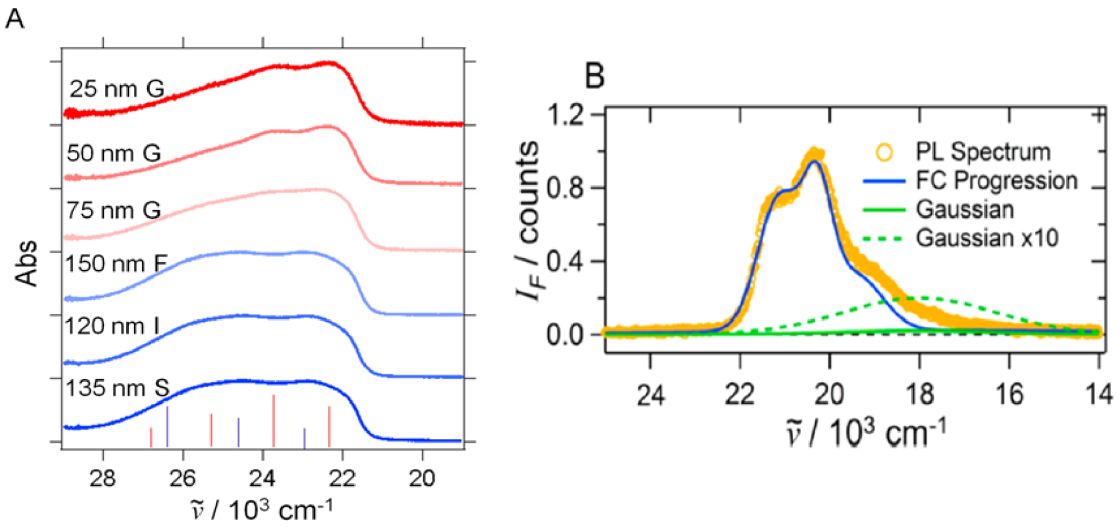

Figure 11. Absorption and fluorescence spectra of thin films of **1**. A: Absorption vs. thickness and substrate type. Blue = type α, red = type β. Substrates are: glass (G), fused silica (F), indium tin oxide (I), and sapphire (S). Stick spectra associated with fit to a Franck-Condon (FC) progression are shown on the horizontal axis. B: Fluorescence for a type β thin film, showing a fit with a FC progression and residual Gaussian shaped emission.

The triplet yields of crystalline thin films of **1** were determined from transient absorption data by taking the ratio of signal amplitudes associated with the maximum triplet signal (Δt = 200 ps) and the initial bleach (Δt = 0.2 ps). This ratio was corrected by the ratio of ground state bleach to triplet absorption molar extinction coefficients at 22500 cm^{-1} and 21500 cm^{-1}, respectively. This ratio was assumed to be ε_G:ε_T = 0.7, the same as in solution. The corrected signal ratio was further modified by an orientation factor that reflects the relative alignment of triplet and S_0-S_1 bleach transition dipole moments at the respective wavelengths. The transition moment of the ground state absorption lies in the molecular *y* axis, and XRD results imply that in thin films it is therefore oriented parallel to the substrate surface. The triplet absorption has a mixed polarization (*y*,*z*) in the spectral region of interest, and only the *y*-polarized fraction contributes significantly to the observed film absorption at normal incidence. Tilting the sample and detecting the triplet signal E^T with s- and p-polarized light as a function of the tilt angle ω yielded no change in triplet absorption strength. The fraction of absorption that is polarized along *y* is given by $2E_{sT}\ \sin^2\omega/[E_p^T - E_s^T(1 - 3\sin^2\omega)]$. Since measurements suggest $E_p^T \simeq E_s^T$, this quantity reduces to 2/3. The two corrections cancel, leaving the ratio of net signal amplitudes for triplet and bleach equal to the triplet yield.

The triplet yield Φ_T for the α form is ~1.4 at room temperature (Figure 12A). It depends on temperature, rising to 2.0 at 80 K before falling slightly by 10 K. It is much smaller for the β form, ~0.1 at room temperature [32]. The dramatic difference in Φ_T between the two forms is underpinned by the kinetic profiles of singlet and triplet state populations determined from transient absorption spectroscopy (Figure 12B). Transition assignments are made using information obtained from solution studies of **1** and are justified by the weak electronic coupling displayed in the films.

In α films, the T_1-T_n absorption features rise with an ~15 ps time constant, which is identical to the decay time constant of stimulated emission and S_1-S_n absorption. Concomitantly, the bleach strength increases with the same time constant, signaling the consumption of additional ground states during SF. The increase in bleach amplitude can be quantified and provides a second estimate of Φ_T, which matches the yield found from direct counting of triplets produced after excitation. For β films, a large stimulated emission component is present from early delay times and decays multiexponentially. A small residual triplet signature is observed at long delay times. We have identified several factors that limit Φ_T for β-type crystals: (i) an intrinsically slower SF process due to lower values of the SF matrix elements as calculated from molecules in the unit cells of α and β, (ii) the propensity for fast excimer formation, and (iii) a larger Davydov splitting that leads to a depressed S_1 energy that introduces a significant unfavorable energy difference between $E(S_1)$ and $2\times E(T_1)$ [61]. Evidence for excimer formation is found in the fast rise of a broadened stimulated emission feature for β films.

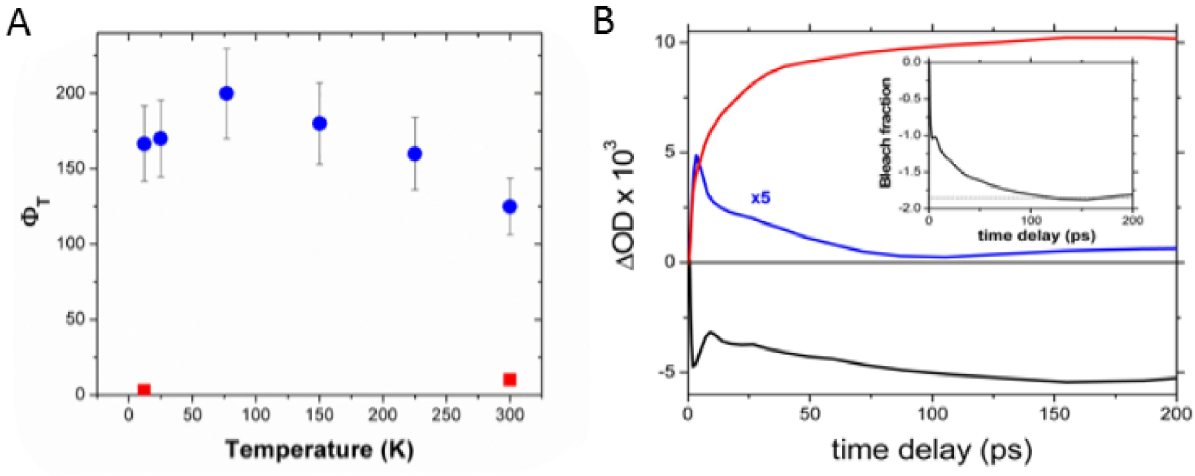

Figure 12. A: Triplet quantum yield vs. temperature for (blue) and (red) films. B: Transient absorption profiles for α film, corresponding to singlet (blue), triplet (red), and ground state bleach (black) populations. Copyright 2010 American Chemical Society.

Crystal engineering strategies have been considered for modulating singlet fission rates, but many intrinsically alter the electronic structure of the molecule to an excessive degree [63]. The series of alkylated[50] and fluorinated[51] derivatives of **1** shown in Figure 3 provides an interesting variety of intermolecular packing geometries in polycrystalline thin films (Figure 13), without significant perturbation of the chromophores and their S_1 - T_1T_1 energy alignment.

Whereas films of the parent **1** and its monofluoro derivative **1a** have nearly identical intermolecular packing and both exhibit a ~15 ps SF rate (Figure 14C shows the associated spectrum), the pentafluoro derivative **1d** with a slightly modified slip-stack structure undergoes SF in ~7 ps[51]. In these instances, S_0 bleach and S_1 and T_1 absorption are the only features observed in the transient absorption spectrum and these times reflect SF rates. The increased rate is most

likely due to a larger slip distance. The crystal structure for the decafluoro derivative **1e** reveals a different packing motif, in which the molecules are not slip-stacked but arranged with their *y* axes close to mutually perpendicular. An excimer is not formed and transient absorption measurements of films of **1e** show that SF still occurs with a time constant of ~12 ps, slightly faster than for **1**.

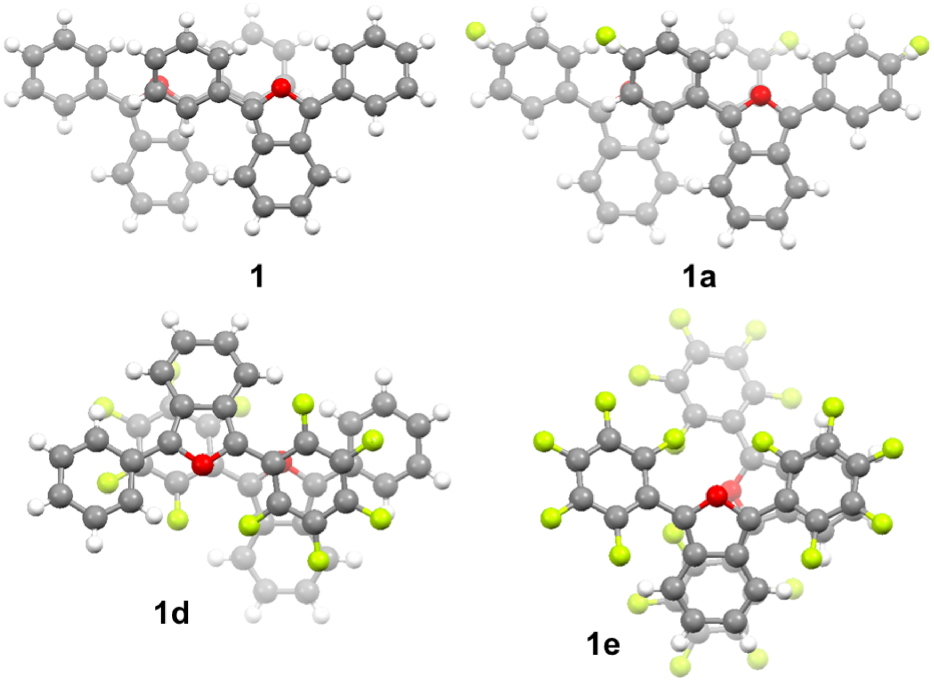

Figure 13. Views of mutual disposition of closest pairs of molecules in selected crystals of **1** and its derivatives. Red spheres represent oxygen, yellow spheres are fluorine, blue spheres are nitrogen, gray spheres are carbon, and white spheres are hydrogen. For **1a** the para substituents are displayed as half hydrogen and half fluorine due to crystal symmetry.

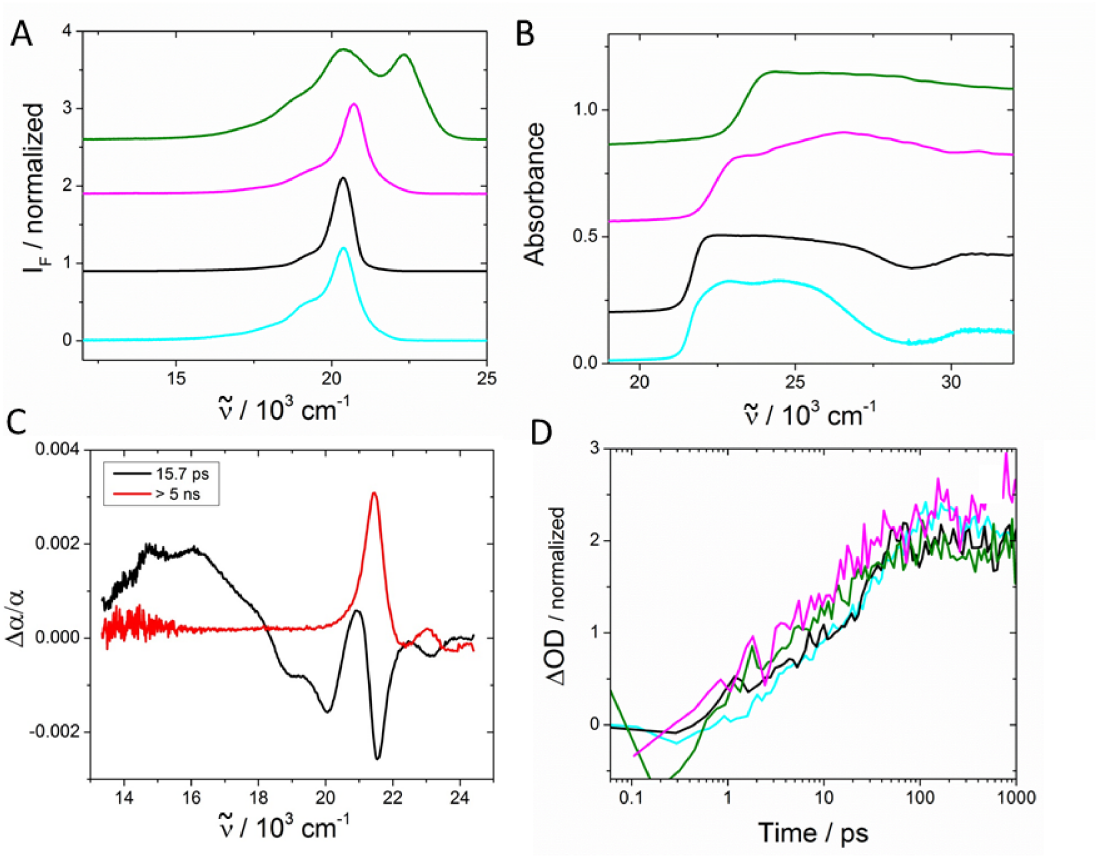

Figure 14. A: Fluorescence and B: UV-VIS absorption for films of fluorinated derivatives of **1** (offset for clarity, **1**, **1a**, **1d**, **1e**, bottom to top). C: Decay associated spectra for a film of **1a**, showing exclusively triplet bands in the long-lived component and mixed singlet/triplet bands corresponding to S_1 - T_1T_1 conversion in the 15 ps component. D: Kinetic profiles of triplet population probed at ~21500 cm^{-1} for **1**, **1a**, **1d**, and **1e**. For color scheme, see A and B.

Derivatives of **1** carrying one or two alkyl (methyl or *tert*-butyl) groups on one of the phenyl rings (**1f- 1h**) have also been investigated[50]. Their absorption and fluorescence spectra in solution are nearly identical with that of **1**, and the fluorescence quantum yields are essentially unity. The films cast from solution are at best partially crystalline, with only **1f** exhibiting clear peaks in XRD. The absorption spectra are slightly broadened compared with solution, most notably for **1g** and **1h**. In all films, two stages of excited state evolution are detected (listed in the order **1f**, **1g**, **1h**): one with ~25, 35, and 75 ps time constants and the other with ~300, 500, and 800 ps (Figure 15A). In each case, triplet formation is most clearly seen in the slower step, while excimer formation occurs with the faster time constant. The relative yields of triplet vs. excimer can be qualitatively discerned by their strengths of absorption (at 21500 cm^{-1} and 18000 cm^{-1}) in the long delay time spectra (Figure 15B). The values of Φ_T are 0.75 ± 0.2, 0.55 ± 0.18, and 0.34 ± 0.15. The parallel formation of excimers and triplets suggests a "two-site" model for excited state dynamics in these quasi-

amorphous films, similar to the behavior found in quasi-amorphous diphenyltetracene films [62], in which slow exciton diffusion to preferred sites leads to a delayed rise in triplets. The trend in triplet formation time and Φ_T for alkyl-substituted **1** is correlated with the substitution of increasingly bulkier groups. The disruption of close packing potentially affects both the concentration of SF active nearest neighbor sites (most prevalent in regions where type α phases are present), as well as the opportunity for fast diffusion to such sites. Excitations residing and remaining at the majority of locations in a disordered film are likely to quickly form excimers.

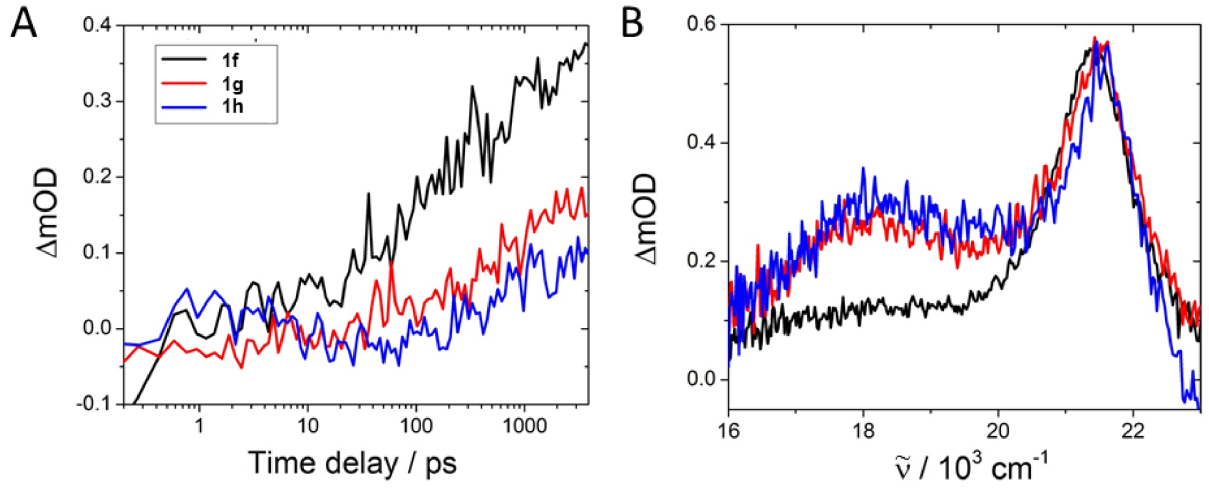

Figure 15. A: Triplet rise profiles of alkyl-substituted derivatives obtained from transient absorption. B: Transient absorption spectra at delay time of 5 ns.

Covalent Dimers of 1

Weakly Coupled Dimers. With two molecules of **1** covalently bound to each other, a range of interchromophore dispositions and electronic couplings has been explored (Figure 16). Weak electronic coupling, needed to avoid excessive triplet-triplet interaction, is assured either by the inclusion of an aliphatic spacer between chromophores, or by enforcing a large twist between dimer halves via steric effects, or by connecting the monomers through their meta positions (**2,3,4**) [63]. In these dimers, excitonic effects slightly modify the solution vibronic envelope of **1**. Additional strength is observed near the lowest 0-0 transition in those dimers that have the *y* axes of **1** (Figure 3) aligned head-to-tail. Molar absorption is approximately doubled in the dimers relative to **1**, as expected for two independent chromophores. Fluorescence remains the dominant excited state pathway for the weakly coupled dimers in nonpolar solvents, with Φ_F in excess of 0.90. Triplets are undetectable after direct excitation ($\Phi_T < 1\%$). The fluorescence lifetimes are slightly reduced compared to **1**, but the spectral features S_1-S_n (obtained by transient absorption after direct excitation) and T_1-T_n (obtained by transient absorption following triplet sensitization) remain unchanged.

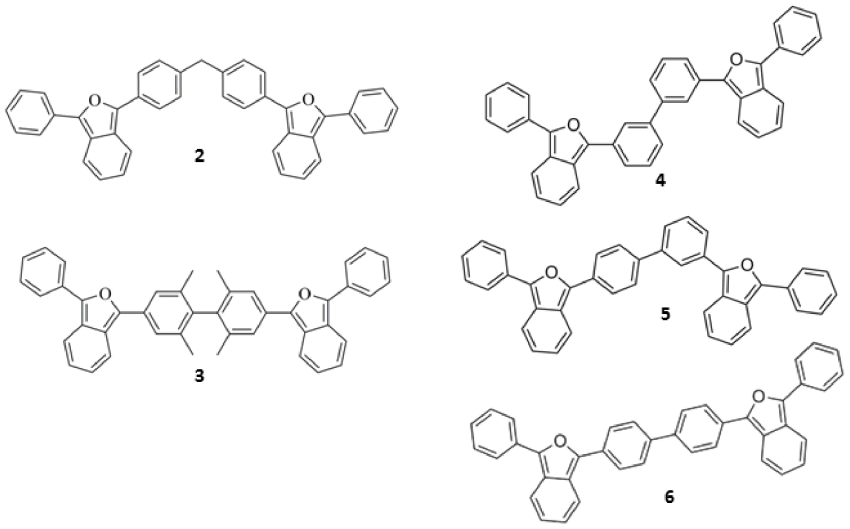

Figure 16. Covalent dimers of **1**.

In polar solution the situation changes dramatically. Φ_F is strongly quenched to a value between 0.1 and 0.3. The fluorescence lifetimes become multiexponential with fast (0.2 ns), intermediate (1-2 ns) and slow (4-6 ns) components (Figure 17A). In pump-probe spectroscopy, absorption bands at 15000 cm^{-1} and 18000 cm^{-1} are observed. Through comparison with the spectra of radical ions of **1** described above, the bands are assigned to $\mathbf{1}^{\bullet+}$ and $\mathbf{1}^{\bullet-}$ and it becomes clear that the charge-separated, or so-called "charge-transfer (CT) state" of the dimer is being observed. The rise time of the CT features characterizes the charge transfer event as relatively fast (50-200 ps) and dependent on the interchromophore geometry and solvent polarity. The CT and S_1 species are in equilibrium and the fluorescence lifetimes thus reflect all of the relevant rates. A small yield of triplet states Φ_T is detected at delay times longer than 1 ns, and the triplet rise time is correlated with CT population decay (Figure 17B). Φ_T varies from 0.01 to 0.10 depending on temperature and solvent. Due to the low yields, a definitive assignment of the triplets as being born from SF is not possible, and radical pair intersystem crossing also is a plausible pathway (Figure 17C). In any event, it is apparent that the SF time is much longer than the natural decay time of the CT state (1-2 ns). A more recent report on a terrylenediimide dimer system comes to similar conclusions about the deleterious effect of populating the real CT state in polar solvents; however, in that case the beneficial involvement of the virtual CT state in nonpolar solvents was also shown [64].

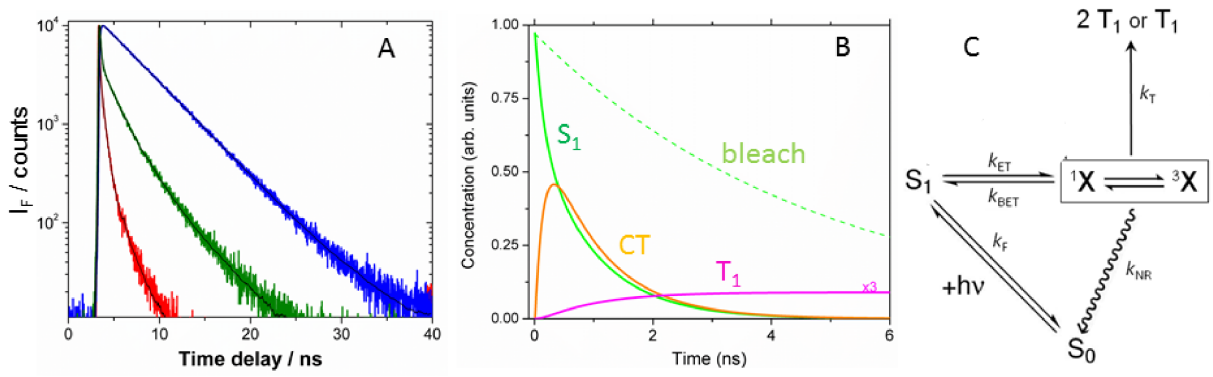

Figure 17. A: Fluorescence decay kinetics for **1** (blue), **2** (red), and **3** (green) in DMSO. B: Concentration profiles from transient absorption showing rise and decay of CT state population correlated with rise of triplet. C: Scheme for triplet formation in **2** and **3** involving intermediate X = CT state. Used with permission from ACS.

Measurement of the temperature dependent rate of charge transfer between halves of the dimer yielded an energy difference between the localized S_1 and CT states of several kcal/mol. Shifting of the S_1-CT equilibrium toward the CT states at lower temperatures forces a shift of additional population to T_1, which increases the triplet quantum yield at lower temperatures. This trend continues as temperature is lowered until charge transfer is arrested as the solvent freezes, and thus solvent stabilization of the CT state upon photoexcitation is too slow to compete with radiative relaxation from S_1. This type of behavior mimics observations of so-called twisted intramolecular charge-transfer states (TICT) in classical systems[65].

Strongly Coupled Dimers. Covalent dimers with stronger electronic coupling have no spacer between chromophores, no substitution for increased steric hindrance, and a para-para or meta-para attachment regiochemistry (**5** and **6**). These directly conjugated dimers behave differently than **1**, even in nonpolar solvents. A red-shifted and broadened ground state absorption is observed, particularly for **6** [66]. Fluorescence is also red-shifted and strongly solvatochromic (Figure 18A), with widely varying yields of 20 - 85%. Fluorescence decay kinetics detected at various wavenumbers are generally biexponential, and the amplitude spectra associated with the faster and slower components are unique. The spectrum associated with the slower decay is blue-shifted and more strongly structured, similar to that of isolated **1**. The spectrum associated with the faster decay is red-shifted, which suggests a species with larger oscillator strength and more extended delocalization than isolated **1**. The corresponding excitation spectra reveal similar trends: a monomer-like excited state species dominates at higher energies whereas evidence for a state with extended conjugation is found at lower energies.

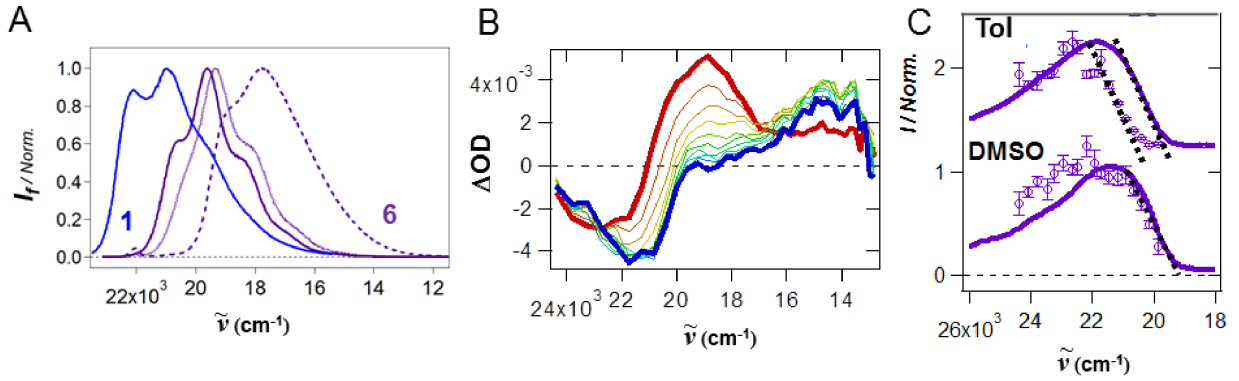

Figure 18. A: Fluorescence of **6** in cyclohexane (solid), toluene (dotted), and DMSO (dashed). Fluorescence of **1** in toluene is shown for comparison. B: Transient absorption spectra of **4** in toluene from delay times of 100 ns (red) through 50 ps (blue). C: Action spectrum for triplet production for **6** in toluene and DMSO.

Triplets form in both polar and nonpolar solvents. For **5**, the triplet yield is 0.08 in toluene and 0.12 in DMSO. In DMSO the triplets clearly form via a CT intermediate state as in **2** and **3**, whereas in toluene the CT state formation is less clear. For **6**, the initially formed triplet spectrum resembles T_1-T_n of **1** with a slight red shift (maximum at ~20000 cm^{-1}). However, over the course of 1-50 ps, the spectrum changes and contains only a strong band at 14000 cm^{-1} (Figure 18B). This strong band is also observed upon triplet energy transfer from anthracene. The action spectrum of triplet formation in toluene, Figure 18C, reveals a shift in the onset of triplet production from that of the ground state absorption, implying a higher energy singlet more efficiently forms triplets than a lower energy singlet. Calculations of minimized singlet and triplet geometries (Figure 19) further point toward a dual triplet model in which a localized triplet resembling that of monomeric **1** forms relatively efficiently (Φ_T ~ 0.30 - 0.40) upon excitation above 22000 cm^{-1}. A delocalized triplet forms with low efficiency (Φ_T < 0.05) after lower energy excitation. The latter triplet is also formed via diffusion controlled energy transfer between the localized triplet and the ground state of **6**.

The excitation localization/delocalization isomerism, present in both the triplet state and the first singlet excited but not the ground state, is quite unusual. It appears to result from the excitation of ground state species with particular geometries favored to produce an excited singlet that is predominantly localized (higher energy excitation) or delocalized (lower energy excitation),cf. Figure 19. These singlets then can produce triplets that are correspondingly localized or delocalized. The excited singlet with twisted geometry is found to be less prevalent when **6** is dissolved in polar solvents, and concomitantly the dual behavior is more difficult to detect (Figure 18C) than in less polar solvents like toluene. SF appears possible from the localized singlet, but it would probably be highly endothermic from the delocalized singlet, which from temperature and excitation energy dependence of fluorescence is found to lie 2300 cm^{-1} below the localized singlet.[67] This type of isomerism may be an important feature of other SF dimer systems, which have gained increasing attention recently [64,68,69].

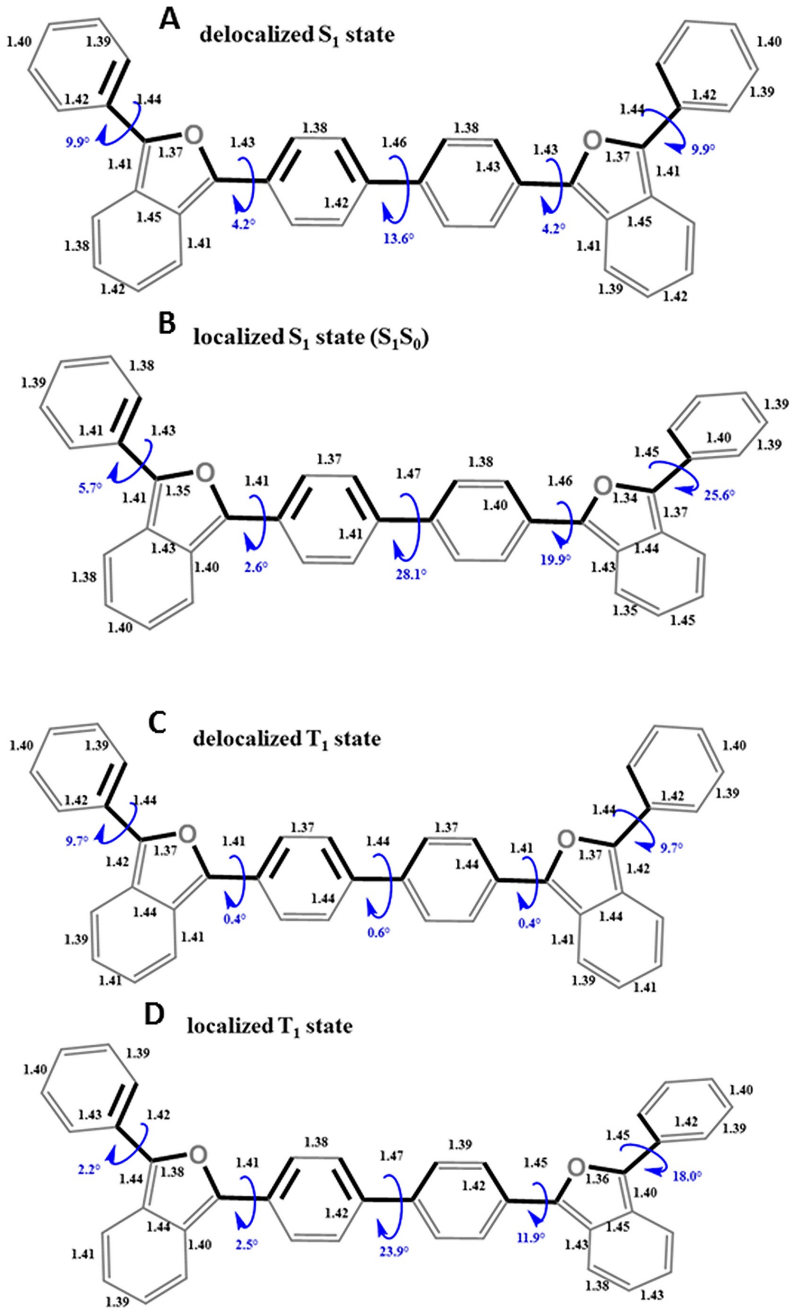

Figure 19: A,B: A comparison of the calculated geometries of the delocalized S_1^* and localized S_0S_1 states for the "syn" conformer of **6** (B3LYP/SVP and TD-HF/SVP, respectively). C,D: A comparison of the calculated geometries of the delocalized T_1^* and localized S_0T_1 states for the "anti" conformer of **6** (B3LYP/SVP and HF/SVP, respectively).

Photovoltaic Devices with the Chromophore 1

In order to observe evidence of SF in a situation where charges are collected, one must couple the SF chromophores to a charge (or energy) acceptor [70]. Dye sensitized solar cells (DSSCs) are common platforms for extracting charge from an organic dye following photoexcitation. We employed **1** and **1n** as "sensitizers" of nanocrystalline TiO_2 for collection of photocurrent [71]. Without functionalization **1** should not have strong affinity for binding to TiO_2; however, we discovered that a small amount of a colorless photo-oxidation product that formed in oxygenated solutions was able to facilitate adsorption of **1** on TiO_2 surface. The sensitized photoelectrodes were brightly colored and stable in an electrolyte (Figure 20A). The devices produced a high yield of photocurrent (roughly 80% internal quantum efficiency) and an overall power conversion efficiency of 1.1%. Electron transport through the nanocrystalline TiO_2 films was found to be on par with that seen in high-performing dye/TiO_2 systems, resulting in diffusion lengths (60-100 μm) that were at least eight times longer than the typical film thickness (~7 μm). Thus, the photocurrent yield was not limited primarily by recombination but rather by the yield of injected charges, which is potentially influenced by SF. However, the electron injection time was measured to be less than 200 fs, far faster than SF.

In order to demonstrate that triplets born from SF could be dissociated and lead to photocurrent, a dielectric barrier of varying thickness was deposited on the TiO_2 surface (Figure 20B). ZrO_2 was deposited via chemical bath deposition in cycles that added ~5 Å of thickness each. The dielectric barrier reduced the electron injection rate from S_1, allowing SF to occur in the chromophore assembly near the surface. Subsequent injection from long-lived triplets, created at a yield of roughly 1.5 times that of singlets, led to a "kink" in the photocurrent vs. barrier thickness profile (Figure 20C). The rise in photocurrent corresponds with the thickness of ZrO_2 needed to slow electron injection from S_1 beyond ~30 ps, the estimated SF time for the molecules near the TiO_2 surface (Figure 20D).

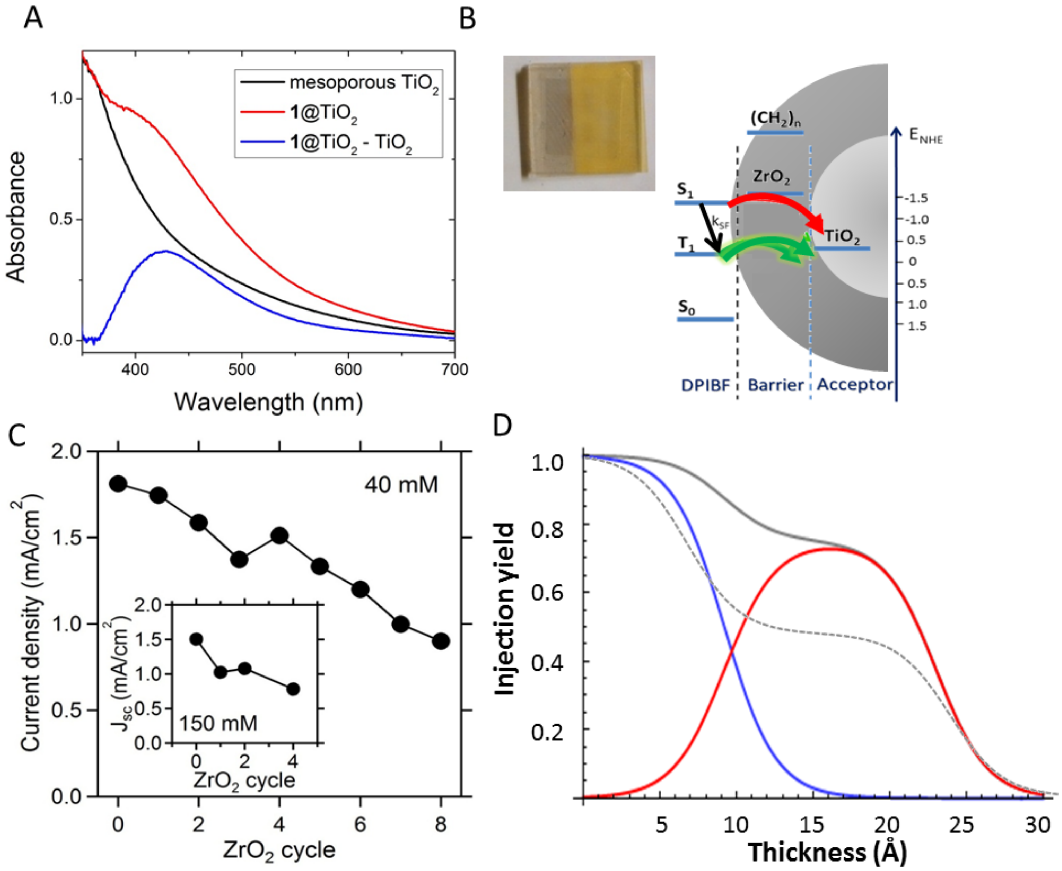

Figure 20. A: Net UV-VIS absorption of **1** on nanocrystalline TiO_2 photoelectrodes. Inset: Photograph of stained TiO_2. B: SF and electron injection scheme with anticipated energy level alignments. C: Photocurrent density vs. ZrO_2 cycle (roughly 5 Å per cycle). D: Calculated photocurrent curve with singlet (blue) and triplet (red) contributions.

A five-carbon saturated chain terminated with a carboxylic acid group was attached to **1** to yield **1n** and covalently bind the dye to the surface. Now, binding was strong even in the absence of the photo-oxidation products, and the carbon chain further slowed the S_1 injection process. The "kink" in the photocurrent spectrum occurred for much smaller thickness of ZrO_2 than with the unsubstituted **1**. The photocurrent quantum efficiency of the device never exceeded 100% due to loss channels that advance with increasing ZrO_2 thickness. However, the clear demonstration of the influence of triplets born from SF on the photocurrent represents an important step toward the practicality of SF based solar photoconversion devices.

Outlook

1,3-Diphenylisobenzofuran (**1**) represents the first successful demonstration of a molecule specifically designed to exhibit efficient SF. The observation of high triplet quantum yield and the

associated fast triplet rise times in thin films has left little doubt about the validity of the design principles used to arrive at small molecule candidate structures based on biradicaloids for SF. The potential for utilizing SF in **1** has also been demonstrated, although true practicality would require further functionalization to endow the chromophore with greater photostability and optical absorption that covers a larger portion of the solar spectrum. In particular, schemes in which triplets born from SF in biradicaloids like **1** undergo energy transfer to high-performing narrow band gap bulk semiconductors should be explored [72,73]. The S_0-T_1 energy gap of **1**, roughly 1.42 eV, is significantly larger than the band gap of Si (1.1 eV), but may be an excellent match for GaAs (~1.4 eV), from which world record single-junction solar cells have been made. This type of very simple tandem solar cell has promise for practical utilization.

Acknowledgments

This material is based on work supported by the U. S. Department of Energy, Office of Basic Energy Sciences, Division of Chemical Sciences, Biosciences, and Geosciences. J.C.J acknowledges Contract No. DE-AC36-08GO28308 with NREL and J.M. acknowledges Award Number DOE DE-SC0007004. J.M. also acknowledges support from the Grant Agency of the Czech Republic, Grant No. GA15-19143S.

References

1. Shockley W, Queisser HJ (1961) J Appl Phys 32:510-519
2. Hanna MC, Nozik AJ (2006) J Appl Phys 100:074510-074518
3. Smith MB, Michl J (2010) Chem Rev 110:6891
4. Smith MB, Michl J (2013) Annu Rev Phys Chem 64:361
5. Buchanan EA, Havlas Z, Michl J (2017) In: Sabin JR, Brändas, EJ (eds) Advances in quantum chemistry: Ratner volume, Vol 17, Academic Press, AIQ, UK.
6. Johnson JC, Michl J (2014) In: Nozik AJ, Conibeer G, Beard MC (eds) Advanced concepts in photovoltaics, Royal Society of Chemistry, Oxfordshire, UK
7. Swenberg CE, Geacintov NE (1973 and 1975) In: Birks JB (ed) Organic molecular photophysics, Vols. 1 (pp. 489 - 564) and 2 (pp. 395 - 408), Wiley, London, UK; Pope M, Swenberg CE (1999) Electronic processes in organic crystals and polymers, 2nd edn. Oxford University Press, Oxford, UK

8. Singh S, Jones WJ, Siebrand W, Stoicheff BP, Schneider WG (1965) J Chem Phys 42:330-342
9. Swenberg CE, Tracy WT (1968) Chem Phys Lett 2:327-328
10. Geacintov NE, Pope M, Vogel F (1969) Phys Rev Lett 22:593-596
11. Pope M, Geacintov NE, Vogel F (1969) Mol Cryst Liquid Cryst 6:83-104
12. Merrifield RE, Aviakan P, Groff RP (1969) Chem Phys Lett 3:386-388
13. Groff RP, Avakian P, Merrifield RE (1970) Phys Rev B 1: 815
14. Tomkiewicz Y, Groff RP, Avakian P (1971) J Chem Phys 54: 4504-4507
15. Geacintov NE, Burgos J, Pope M, Strom C (1971) Chem Phys Lett 11:504-508
16. López-Delgado R, Miehé JA, Sipp B (1976) Opt Commun 19:79-82
17. Yarmus L, Rosenthal J, Chopp M (1972) Chem Phys Lett 16:477-481
18. Swenberg CE, Van Metter R, Ratner M (1972) Chem Phys Lett 16:482-485
19. Swenberg CE, Geacintov NE (1973) In: Birks JB (ed) Organic molecular photophysics, Wiley, New York
20. Klein G, Voltz R, Schott M (1972) Chem Phys Lett 16:340-344
21. Klein G, Voltz R, Schott M (1973) Chem Phys Lett 19:391-394
22. Arnold S, Alfano RR, Pope M, Yu W, Ho P, Selsby R, Tharrats J, Swenberg CE (1976) J Chem Phys 64:5104-5114
23. Fleming GR, Millar DP, Morris GC, Morris JM, Robinson GW (1977) Aust J Chem 30:2353-2359
24. Frankevich EL, Lesin VI, Pistupa AI (1978) Chem Phys Lett 58:127-131
25. Von Burg K, Zchokke-Gränacher I (1979) J Chem Phys 70:3807-3811
26. Arnold S, Whitten WB (1981) J Chem Phys 75:1166-1169
27. Katoh R, Kotani M (1992) Chem Phys Lett 196:108-112

28. Jundt C, Klein G, Sipp B, Le Moigne J, Joucla M, Villaeys AA (1995) Chem Phys Lett 241:84-88
29. Müller AM, Avlasevich YS, Müllen K, Bardeen CJ (2006) Chem Phys Lett 421:518-522
30. Müller AM, Avlasevich YA, Schuller WW, Müllen K, Bardeen CJ (2007) J Am Chem Soc 129:14240-14250
31. Lee J, Jadhav P, Baldo MA (2009) Appl Phys Lett: 95:192
32. Johnson JC, Nozik AJ, Michl J (2010) J Am Chem Soc 132:16302-16303
33. Wang C, Tauber MJ (2010) J Am Chem Soc 132:13988-13991
34. Burdett JJ, Müller AM, Gosztola D, Bardeen C (2010) J Chem Phys 133:144506
35. Paci I, Johnson JC, Chen X, Rana G, Popović D, David DE, Nozik AJ, Ratner MA, Michl J (2006) J Am Chem Soc 128:16546-16553
36. Herkstroeter WG, Merkel PB (1985) J Photochem 16:331-341
37. Ziebig R, Pragst FZ (1979) Z Phys Chem 260:795-803
38. Howard JA, Mendenhall GD, (1975) Can J Chem 53:2199-2201
39. Krieg M (1993) J Biochemical and Biophysical Methods 27:143-149
40. Minami T, Nakano M (2012) J Phys Chem Lett 3:145-150
41. Akdag A, Havlas Z, Michl J (2012) J Am Chem Soc 134:14624-14631
42. Zeng T, Ananth N, Hoffmann R (2014) J Am Chem Soc 136:12638-12647
43. aminoquinone biradicaloids Jin Wen
44. Johnson JC, Nozik AJ, Michl J (2013) Acc Chem Res 46:1290-1299
45. Feng XT, Luzanov AV, Krylov AI (2013) J Phys Chem Lett 4:3845-3852
46. The only exception that we are aware of is a claim that for two stacked tetracenes slipped strongly along the long axis and only slightly along the short axis the direct term dominates completely over the mediated term: Tamura H, Huix-Rotllant M, Burghardt I, Olivier Y,

Beljonne, D. (2015) Phys Rev Lett 115:107401. We have been unable to reproduce this result within the HOMO/LUMO model and find that this case is unexceptional in that the mediated term exceeds the direct term by more than two orders of magnitude.

47. Havlas Z, Michl J (2016) Isr J Chem 56:96-106
48. Ryerson J, Schrauben JN, Ferguson AJ, Sahoo SC, Naumov P, Havlas Z, Michl J, Nozik AJ, Johnson JC (2014) J Phys Chem C 118: 12121-12132
49. Teichen PE, Eaves JD (2015) J Chem Phys 143:044118
50. Dron PI, Schrauben JN, Akdağ A, Michl J, Johnson JC, submitted for publication.
51. Kaleta J, Buchanan EA, Císařová I, Johnson JC, Michl J, unpublished results.
52. Akdag A, Wahab A, Beran P, Rulíšek L, Dron PI, Ludvík J, Michl J (2015) J Org Chem 80:80-89
53. Jacq J, Einhorn C, Einhorn J (2008) Org Lett 10:3757-3760
54. Schwerin AF, Johnson JC, Smith MB, Sreearunothai P, Popović D, Černý J, Havlas Z, Paci I, Akdag A, MacLeod MK, Chen X, David DE, Ratner Ma, Miller JR, Nozik AJ, Michl J (2010) J Phys Chem A 114:1457-1473
55. Platt JR (1949) J Chem Phys 17:484-495
56. Moffitt W (1954) J Chem Phys 22:320-333 and 22:1820-1829
57. Michl J (1984) Tetrahedron 40: 3845-3934
58. Nelsen SF, Weaver MN, Yamazaki D, Komatsu K, Rathore K, Rathore R, Bally T (2007) J Phys Chem 111:1667-1676
59. Dillon RJ, Piland GB, Bardeen CJ (2013) J Am Chem Soc 135:17278-17281
60. Margulies EA, Logsdon JL, Miller CE, Ma L, Simonoff E, Young RM, Schatz GC, Wasielewski MR (2016) J Am Chem Soc. Doi:10.1021/jacs.6b07721
61. Schrauben J, Ryerson J, Michl J, Johnson J (2014) J Am Chem Soc 136:7363-7373

62. Roberts ST, McAnally RE, Mastron JN, Webber DH, Whited MT, Brutchey RL, Thompson ME, Bradforth SE (2012) J Am Chem Soc 134:6388-6400

63. Johnson JC, Akdag A, Zamadar M, Chen X, Schwerin AF, Paci I, Smith MB, Havlas Z, Miller JR, Ratner MA, Nozik AJ, Michl J (2013) J Phys Chem B 117:4680-4695

64. Margulies EA, Miller CE, Wu Y, Ma L, Schatz GC, Young RM, Wasielewski MR (2016) Nat Chem 8:1120-1125

65. Grabowski ZR, Rotkiewicz K, Rettig W (2003) Chem Rev 103:3899-4032

66. Schrauben J, Akdag, A, Wen J, Ryerson J, Havlas Z, Michl J, Johnson JC (2016) J Phys Chem A 120:3473-3483

67. Greyson EC, Stepp BR, Chen X, Schwerin AF, Paci I, Smith MB, Akdag A, Johnson JC, Nozik AJ, Michl J, Ratner MA (2010) J Phys Chem B 114:14223-14232

68. Sanders SN, Kumarasamy E, Pun AB, Trinh MT, Choi B, Xia J, Taffet EJ, Low JZ, Miller JR, Roy X, Zhu XY (2015) J Am Chem Soc 137:8965-8972

69. Lukman S, Chen K, Hodgkiss JM, Turban DHP, Hine NDM, Dong S, Wu J, Greenham NC, Musser AJ (2016) Nat Commun 7:13622

70. Congreve DN, Lee JY, Thompson NJ, Hontz E, Yost SR, Reusswig PD, Bahlke ME, Reineke S, Van Voorhis T, Baldo MA (2013) Science 340: 334-337

71. Schrauben JN, Zhao Y, Mercado C, Dron PI, Ryerson JM, Michl J, Zhu K, Johnson JC (2015) ACS Appl Mater Interfaces 7:2286-2293

72. Tabachnyk M, Ehrler B, Gelinas S, Bohm ML, Walker BJ, Musselman KP, Greenham NC, Friend RH, Rao A (2014) Nat Mater 13:1033-1038

73. Thompson NJ, Wilson MW, Congreve DN, Brown PR, Scherer JM, Bischof TS, Wu M, Geva N, Welborn M, Van Voorhis T, Bulović V (2014) Nat Mater 13:1039-1043